SUPPLEMENT: An Observational Perspective on Precipitation Efficiency of Mesoscale Convective Systems over the Asian Monsoon Region

Thabo Makgoale[1], Sylvia Sullivan[1,2], and Julia Kukulies[3]

[1]Department of Hydrology and Atmospheric Sciences, University of Arizona, Tucson, Arizona, USA
[2]Department of Chemical & Environmental Engineering, The University of Arizona, Tucson, AZ
[3]Mesoscale and Microscale Meteorology Laboratory, NCAR, Boulder, CO, USA

Correspondence: Thabo Makgoale (temakgoale@arizona.edu) and Sylvia Sullivan (sylvia@arizona.edu)

Supporting Information

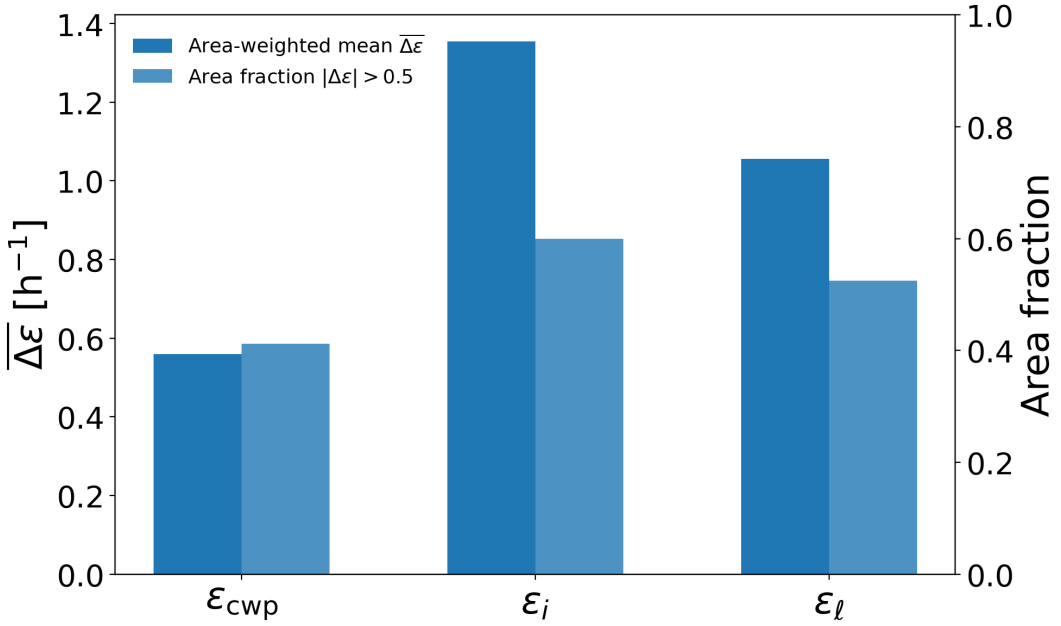

Figure S1. *Ice-phase efficiency (ϵ_i) exhibits both a larger domain-mean enhancement and broader spatial coverage than ϵ_ℓ.* Bars chart show the area-weighted mean difference $\overline{\Delta\epsilon} = \epsilon_{\mathrm{MCS}} - \epsilon_{\mathrm{nonMCS}}$ (left axis) and the fractional spatial coverage where the magnitude of the difference exceeds a physically meaningful threshold ($|\Delta\epsilon| > \tau$, right axis) for cloud water path efficiency (ϵ_{cwp}), ice-phase efficiency (ϵ_i), and liquid-phase efficiency (ϵ_ℓ). Area weighting is applied using $\cos(\phi)$.

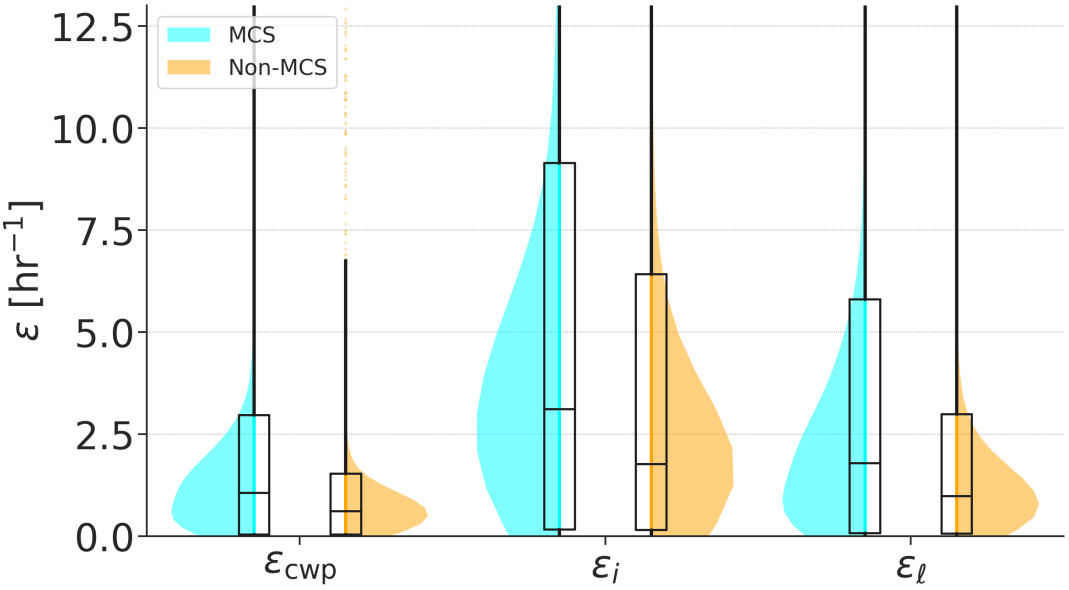

Figure S2. *MCSs have substantially higher ϵ across all phases, with median ϵ values roughly double those of non-MCS convection.* For readability, only one half of each violin distribution is displayed; this half-violin style prevents overlap between MCS (cyan) and non-MCS (orange) distributions. From left to right, box plots show overall total precipitation efficiency (ϵ_{cwp}), ice-phase precipitation efficiency (ϵ_i), and liquid-phase precipitation efficiency (ϵ_l). The boxes indicate the interquartile range, the horizontal line marks the median, and the violin width denotes data density. Whiskers extend to the 5st and 95th percentiles.

Table 1. Pearson correlation coefficients (r) and associated p-values for the relationship between precipitation efficiency (ϵ_{cwp}, ϵ_ℓ, ϵ_i) and MCS area, stratified by microphysical phase, for both mean rain rate and maximum rain rate. All correlations are statistically significant at the 95% confidence level ($p < 0.05$).

Rain-rate metric	**Efficiency component**	r	p**-value**
Mean	ϵ_{cwp}	0.9835	1.11×10^{-5}
	ϵ_ℓ	0.9847	8.84×10^{-6}
	ϵ_i	0.9789	2.32×10^{-5}
Max	ϵ_{cwp}	0.9512	2.81×10^{-4}
	ϵ_ℓ	0.9539	2.36×10^{-4}
	ϵ_i	0.9467	3.63×10^{-4}

Table 2. Pearson correlation coefficients (r) and associated p-values for the relationship between precipitation efficiency (ϵ_{cwp}, ϵ_ℓ, ϵ_i) and brightness temperature (Tb), stratified by microphysical pathway and rain-rate metric. Results are shown separately for mean and maximum rain rates. All correlations are statistically significant at the 95% confidence level ($p < 0.05$).

Rain-rate metric	**Efficiency component**	r	p**-value**
Mean	ϵ_{cwp}	-0.9752	3.74×10^{-5}
	ϵ_ℓ	-0.9786	2.41×10^{-5}
	ϵ_i	-0.9880	4.27×10^{-6}
Max	ϵ_{cwp}	-0.9930	8.68×10^{-7}
	ϵ_ℓ	-0.9894	2.95×10^{-6}
	ϵ_i	-0.9921	1.21×10^{-6}

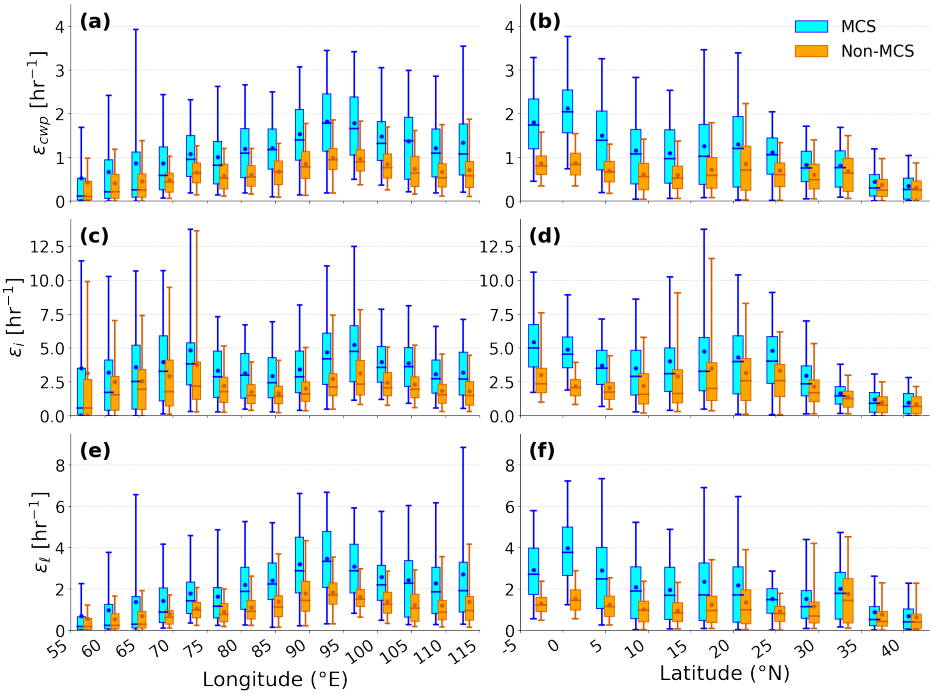

Figure S3. *ϵ tends to increase from west to east and from north to south across our domain, especially in the ice phase.* Boxplots showing the longitudinal (left column) and latitudinal (right column) variations in ϵ for MCSs in cyan and non-MCS convection in orange across the Asian monsoon domain. The top row (a–b) shows overall precipitation efficiency (ϵ_{cwp}), the middle row (c–d) ice-phase precipitation efficiency (ϵ_i), and the bottom row (e–f) liquid-phase precipitation efficiency (ϵ_ℓ). Boxes denote the interquartile range, horizontal lines the median, dots the mean, and whiskers the 5th to 95th percentiles.

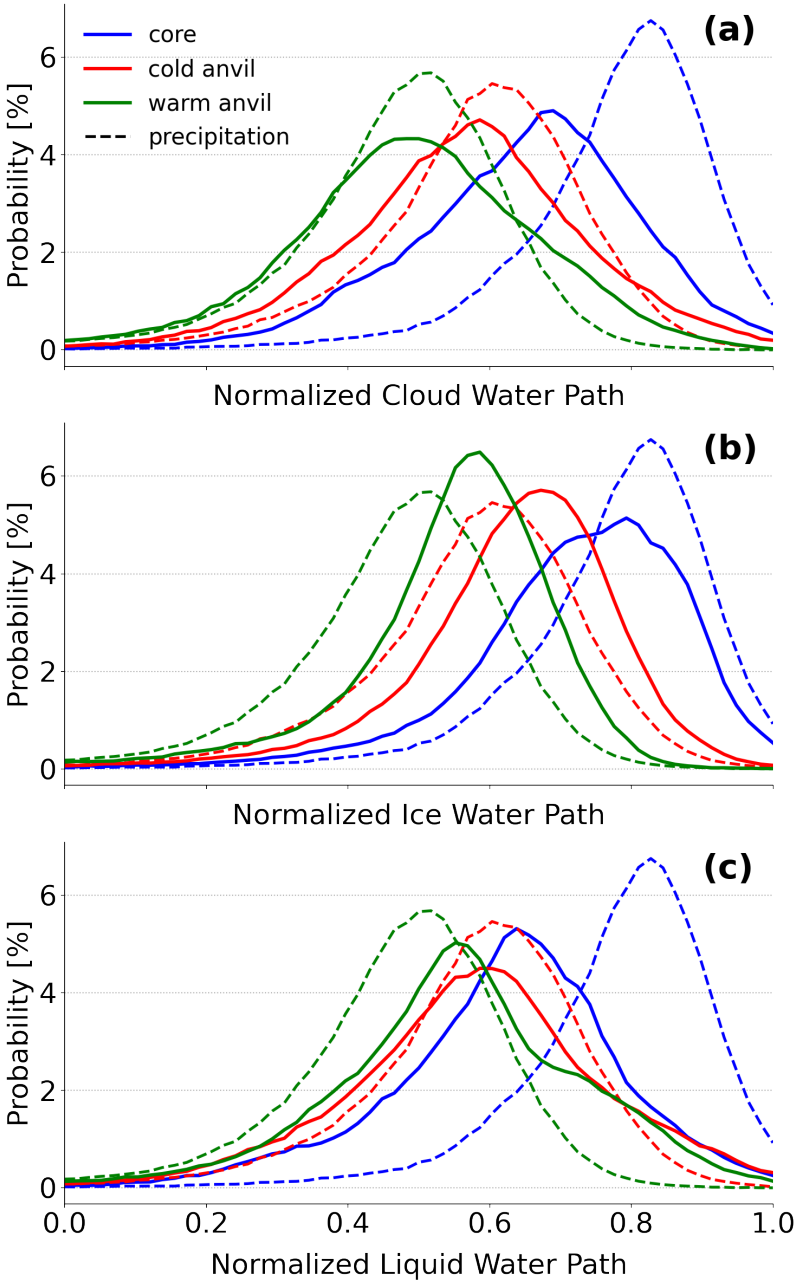

Figure S4. *Precipitation is systematically shifted toward higher normalized values than condensate within core of MCS for all three condensate metrics* Normalized probability distributions comparing column-integrated cloud condensate (solid lines) and precipitation (dashed lines) across three MCS sub-regions over the Asian monsoon domain for 9 Aug–9 Sep 2016. Panels show (a) cloud water path (CWP), (b) ice water path (IWP), and (c) liquid water path (LWP) for the convective core (blue), cold anvil (red), and warm anvil (green). For each variable, distributions are computed from all valid grid cells after removing missing values and are expressed as probability (%). The horizontal axis is a 0–1 normalized coordinate obtained by log-transforming bin centers and scaling to the range of each variable.

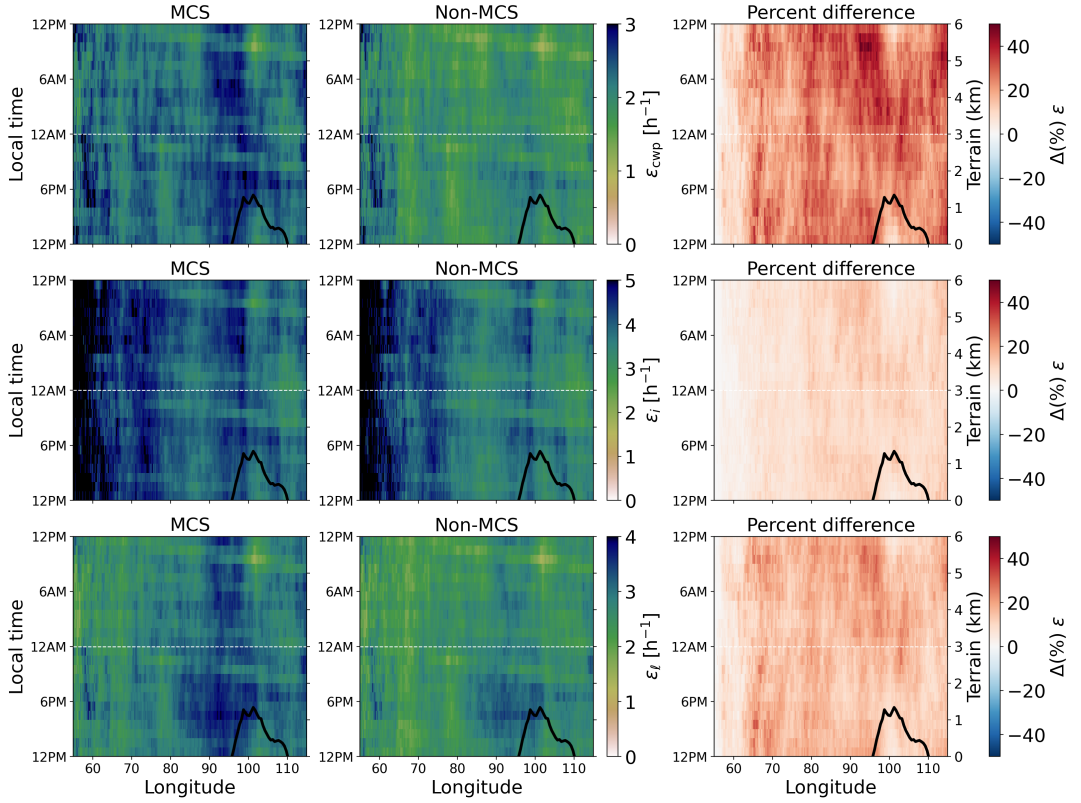

Figure S5. *Topography influenced MCSs show stronger diurnal contrasts in precipitation efficiency (ϵ).* Diurnal Hovmöller diagrams of ϵ, as a function of longitude and local time over the Asian monsoon domain. Rows show ϵ computed using column-integrated condensate metrics: cloud water path (ϵ_{cwp}; top), column ice water (ϵ_i; middle), and column liquid water (ϵ_ℓ; bottom). Columns show the mean diurnal cycle of MCS conditions (left), non-MCS conditions (middle), and the percentage difference $\Delta\epsilon = 100\,(\epsilon_{\mathrm{MCS}} - \epsilon_{\mathrm{nonMCS}})/\epsilon_{\mathrm{nonMCS}}$.